ACS APPLIED MATERIALS & INTERFACES

Research Article

www.acsami.org

Enhanced Tribological, Corrosion, and Microstructural Properties of an Ultrathin (<2 nm) Silicon Nitride/Carbon Bilayer Overcoat for High Density Magnetic Storage

Reuben J. Yeo,[†] Neeraj Dwivedi,[†] Ehsan Rismani,[†] Nalam Satyanarayana,[†] Shreya Kundu,[†] Partho S. Goohpattader,[†] H. R. Tan,[‡] Narasimhan Srinivasan,[§] Boris Druz,[§] S. Tripathy,[‡] and C. S. Bhatia*[,†]

[†]Department of Electrical and Computer Engineering, National University of Singapore, Singapore 117583

[‡]Institute of Materials Research and Engineering (IMRE), A*STAR (Agency for Science, Technology, and Research), 3 Research Link, Singapore 117602

[§]Veeco Instruments Inc, Terminal Drive Plainview, New York 11803, New York, United States

ABSTRACT: An ultrathin bilayer overcoat of silicon nitride and carbon (SiN_x/C) providing low friction, high wear resistance, and high corrosion resistance is proposed for future generation hard disk media. The 16 Å thick SiN_x/C overcoat consists of an atomically thin SiN_x underlayer (4 Å) and a carbon layer (12 Å), fabricated by reactive magnetron sputtering and filtered cathodic vacuum arc (FCVA), respectively. When compared with monolithic overcoats of FCVA-deposited carbon (16 Å) and sputtered SiN_x (16 Å), the SiN_x/C bilayer overcoat demonstrated the best tribological performance with a coefficient of friction < 0.2. Despite showing marginally less electrochemical corrosion protection than monolithic SiN_x, its ability to protect the magnetic media from corrosion/oxidation was better than that of an ~27 Å thick commercial hard disk overcoat and 16 Å thick monolithic FCVA-deposited carbon. From X-ray photoelectron spectroscopy and Raman spectroscopy analyses, it was found that the introduction of the 4 Å SiN_x underlayer facilitated higher sp^3 hybridization within the carbon layer by acting as a barrier and promoted the formation of strong bonds at the SiN_x/C and the SiN_x/media interfaces by acting as an adhesion layer. The higher sp^3 carbon content is expected to improve the thermal stability of the overcoat, which is extremely important for future hard disk drives employing heat assisted magnetic recording (HAMR).

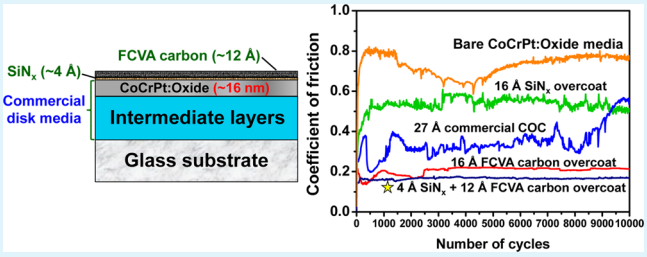

KEYWORDS: *head−disk interface, carbon overcoat, corrosion protection, surface modification, silicon nitride*

1. INTRODUCTION

Commercial hard disk drives (HDDs) today contain a Co-alloy-based magnetic recording media which is used to store digital information. To protect the media from mechanical wear and oxidation, the media is coated with a thin, hard, and chemically inert layer of diamond-like carbon (DLC), which is topped with a monolayer of lubricant to achieve low friction at the head−disk interface. To achieve higher areal densities, the spacing between the magnetic media and the read head, known as the magnetic spacing, has to be further reduced.[1−3] This has motivated a continuous decrease in the DLC overcoat thickness. Future generation HDDs with areal densities > 1 Tb/in^2 require a protective overcoat thickness of <2.0 nm over the hard disk magnetic media.[4] Below this thickness, conventional DLC deposition methods such as ion beam deposition, plasma enhanced chemical vapor deposition (PECVD), and magnetron sputtering[5] bring about many tribological and corrosion-related challenges. Furthermore, heat-assisted magnetic recording (HAMR) is seen as one of the magnetic recording technologies which could be implemented in future high density HDDs.[4,6] In HAMR, the media would be subjected to high temperatures (>500 °C) and rapid thermal cycling rates. Hence, the thermal stability of the protective overcoat is also one of the important issues that need to be addressed.

Filtered cathodic vacuum arc (FCVA) is one of the techniques which can deposit carbon overcoats (COCs) on media with enhanced protective characteristics, low surface roughness, and good film coverage even at lower thicknesses.[7−10] FCVA generates a highly ionized plasma (~90%) of energetic C^+ ions, which helps to achieve a high amount of sp^3 hybridization of carbon within the COC. The high sp^3 carbon (sp^3C) fraction directly contributes to its hardness, elastic modulus, density, and wear resistance, and indirectly contributes to its coverage excellence.[9,11] In addition, FCVA-deposited COC on magnetic media has demonstrated higher thermal stability as compared to a conventional PECVD deposited hydrogenated COC (the thicknesses of the COCs

Received: March 24, 2014
Accepted: May 29, 2014
Published: May 29, 2014

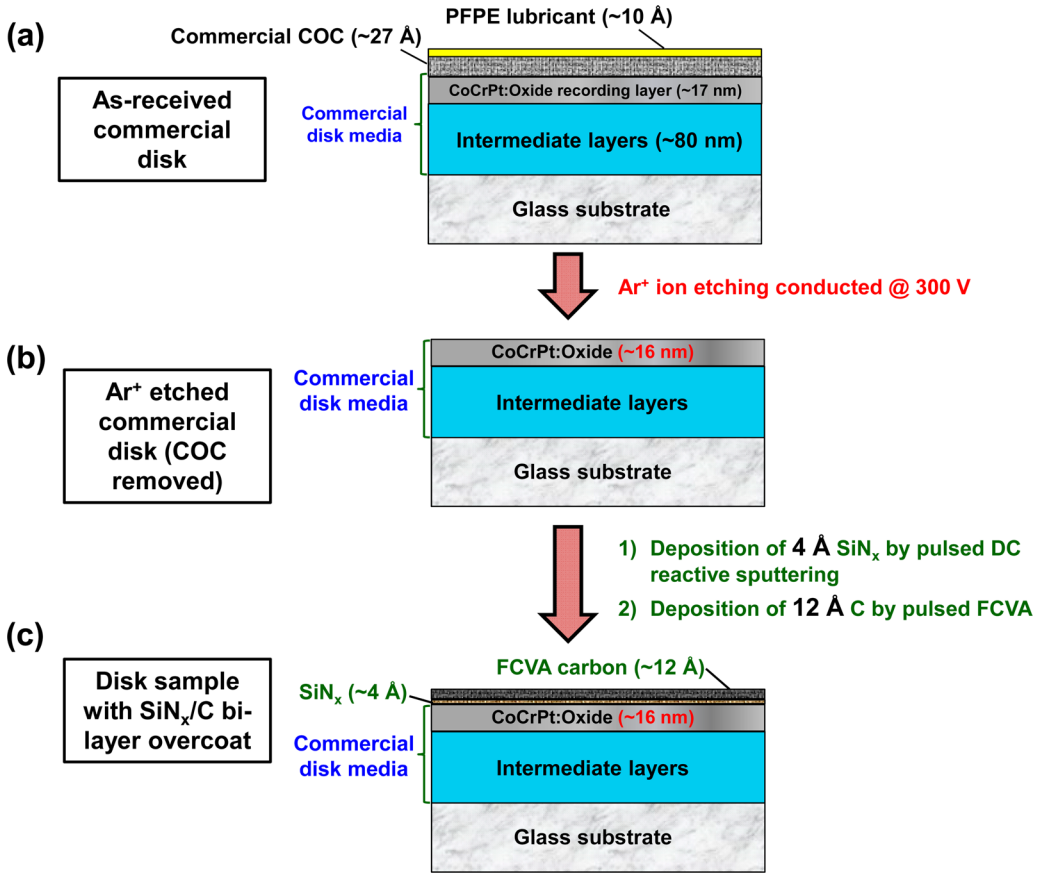

Figure 1. Flowchart showing the surface modification process and cross section schematics of (a) the as-received commercial disk; (b) commercial disk after Ar^+ ion etching for COC removal; and (c) disk sample after deposition of the SiN_x/C bilayer overcoat onto the etched commercial disk.

studied was >3.5 nm).[12,13] The higher thermal stability of the FCVA-deposited COC, which is non-hydrogenated, has been attributed to the higher sp^3C fraction which can be obtained by the FCVA deposition technique. As such, it can be seen that the advantage of the FCVA deposition technique lies in its ability to attain a high sp^3C fraction, which provides all the desirable yet essential qualities for future hard disk media overcoats.

However, at ultrathin levels, FCVA-deposited carbon films show significantly lower sp^3C content as compared to its thicker counterparts. For example, while FCVA-deposited carbon can have up to ~85% sp^3C content for 200 nm films,[14] Ferrari has suggested that FCVA-deposited carbon films achieve only ~50% sp^3C content at ~2 nm thickness.[15] Hence, for overcoat thickness < 2 nm, maintaining or improving the sp^3C fraction and its associated properties (in terms of its good wear resistance, corrosion resistance, and thermal stability) even with FCVA-deposited carbon would be very challenging.

Apart from high sp^3C content, high interfacial strength/bonding at the magnetic media−overcoat interface is also needed for enhanced tribological properties and wear protection. By controlling the C^+ ion energy using the FCVA technique, surface modification of the magnetic media had been performed to obtain an ultrathin graded protective overcoat (≤2.0 nm) by forming a mixed interfacial layer of carbon and media.[16,17] This graded overcoat structure was seen to improve the interfacial bonding between the COC and media, and exhibited a low coefficient of friction even without a lubricant layer. However, the overcoat fabricated by this FCVA surface modification technique has not been found to improve the corrosion performance over commercial hard disks.[18]

The addition of an underlayer is another method of improving the interfacial bonding and adhesion. Rismani et al. found that the addition of a Si underlayer for FCVA-deposited carbon overcoats on Co magnetic media formed interfacial Co−Si and Si−C bonds, giving a better wear durability of the overcoat.[19] Amorphous silicon nitride (SiN_x) films are commonly known for their high hardness, high electrical resistivity, chemical inertness, and good diffusion barrier properties owing to their dense, covalently bonded structure.[20] Furthermore, when used as an underlayer, they have been reported to provide good adhesion between DLC and metallic substrates.[21] However, SiN_x itself is not as wear resistant as DLC, and it is prone to oxidation in ambient oxygen and humidity, especially at low thicknesses.[22,23] Recently, Bunnak et al. prepared 10 nm thick composite SiN_x/DLC films on Si substrates by combining RF sputtering and FCVA deposition techniques, and have observed promising properties in terms of high sp^3 carbon bonding.[24]

By combining the ideal properties of SiN_x and FCVA-deposited carbon, the aim of this study is as follows: (1) to maintain or improve the sp^3C bonding within the COC; (2) to provide good overcoat adhesion to the underlying magnetic media; and most importantly (3) to enhance the tribological properties and corrosion resistance of the overcoat. Here in this work, a SiN_x/C bilayer overcoat is developed with a total thickness of ~16 Å showing remarkable properties. To demonstrate the superiority of the SiN_x/C bilayer overcoat, a monolithic SiN_x overcoat and a monolithic FCVA-deposited carbon overcoat (both with thickness of ~16 Å) were also prepared to compare their properties.

2. MATERIALS AND METHODS

2.1. Sample Preparation. Figure 1 describes the sample preparation process for fabricating the SiN_x/C bilayer overcoat on commercial media disks. Commercial 2.5″ disks were used as the starting substrates in this work, consisting of (from bottom to top) a glass disk substrate, a multilayer structure of various materials for optimized recording performance, a CoCrPt:Oxide magnetic recording layer, a COC layer, and finally a lubricant layer. A cross section schematic of the commercial disk structure is provided in Figure 1a. Prior to deposition of the SiN_x/C overcoat, the pre-existing commercial COC and lubricant layer were removed by Ar^+ ion beam etching at an ion energy of 300 eV, as seen in Figure 1b. A secondary ion mass spectrometer (SIMS) detector was used to calibrate the etching rate to remove the commercial COC. It should be noted that this etching process was applied as a necessary step when fabricating these overcoats for our experiments. However, it is not required in a conventional hard disk manufacturing process.

Deposition of the SiN_x and carbon films on the etched commercial disk substrates were carried out in situ after etching, using a VEECO deposition system equipped with a pulsed filtered cathodic arc source, sputtering source, and Ar^+ ion beam etching capability. A 99.99% pure silicon target was used for the deposition of SiN_x, while a 99.999% pure graphite rod was used for the deposition of carbon by FCVA. Deposition was carried out at a background pressure of $\sim 10^{-7}$ Torr. First, a 4 Å ultrathin layer of SiN_x was deposited by pulsed DC reactive sputtering in a gaseous mixture of Ar + N_2, with a ratio of 67% Ar to 33% N_2 and at a duty cycle of 0.7. Next, the sample was transferred to the FCVA chamber in situ under vacuum. A schematic of a FCVA setup for deposition of COC is shown in Figure 2. A 12 Å layer of carbon was subsequently deposited above the SiN_x layer by pulsed FCVA deposition, giving a total overcoat thickness of 16 Å. During the FCVA deposition process, an arc was struck between the anode and cathode using a high current pulsed power supply with a duty cycle of 0.001. The resulting arc discharge was transported using a single 90° bend filter coil which magnetically confines and guides the plasma toward the substrate. This filter helps to remove any neutrals or macroparticles in the plasma which do not react with the coil's magnetic field. The plasma exiting the filter coil then passes through a plasma shaping coil before reaching the substrate. No substrate bias was applied during the FCVA deposition process, and hence, the average energy of the C^+ ions arriving at the substrate was around 25 eV.[25] The deposition rates of both the sputtered SiN_x and FCVA-deposited carbon layers were calibrated individually by X-ray reflectivity (XRR). The deposition rate of carbon by FCVA was found to be 0.063 Å/pulse. By adjusting the number of pulses, the COCs of desired thicknesses were deposited in samples 16C and 4SiN12C. In addition, the etching rate uniformity as well as the thickness uniformity of the SiN_x and C films were qualified prior to deposition.

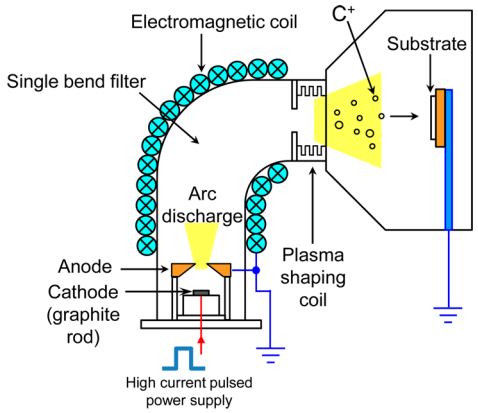

Figure 2. Schematic of a typical FCVA setup for the deposition of COC.

The schematic of the resultant disk sample is shown in Figure 1c. For the purpose of evaluating the performance of the SiN_x/C bilayer overcoat, single layer overcoats of reactive sputtered SiN_x and FCVA-deposited carbon, each with thickness of 16 Å, were also deposited on similar etched magnetic media substrates. The performance of each of these samples was compared to a reference commercial media disk sample with its commercial COC but without the lubricant layer. For completeness, a specially prepared commercial disk without any protective overcoat over the magnetic media was also used in this study to provide a benchmark to show the effectiveness of using a protective overcoat on commercial magnetic media. A list of the samples and their nomenclature (which will be used henceforth) is presented in Table 1.

Table 1. Description and Nomenclature of Samples Used in This Work

nomenclature	sample type	overcoat structure
16C	Ar^+ etched commercial disk (COC removed)	C (16 Å)
16SiN	Ar^+ etched commercial disk (COC removed)	SiN_x (16 Å)
4SiN12C	Ar^+ etched commercial disk (COC removed)	SiN_x (4 Å)|C (12 Å)
CM	as-received commercial disk (without lube)	commercial COC (~27 Å)
BM	as-received commercial disk (without COC and without lube)	no overcoat (bare media)

2.2. Characterization Methods. High resolution cross-sectional transmission electron microscopy (TEM, Philips FEG CM300) was performed to image the microstructure and thickness of the overcoats after deposition. Before imaging, all samples (16C, 16SiN, 4SiN12C, and CM) were prepared for cross-sectional TEM measurements.

To investigate any surface modification induced changes in the smoothness of the media surface, the surface roughnesses of samples S-1 to S-4 were measured with the help of tapping mode atomic force microscopy (AFM, Bruker Innova). The measurements were conducted at a scan area of 2 μm × 2 μm at three different points on each sample surface, from which a mean value was taken.

One of the methods to explore the wear resistance of the overcoats on magnetic media is to investigate their tribological properties through ball-on-disk tribological tests. Ball-on-disk tribological tests were carried out on all the samples using a nanotribometer (CSM Instruments). Sapphire (Al_2O_3) was used as the counterface ball material, and a contact load of 20 mN (the minimum load which can be applied by the tribometer) was kept constant in all the tests. The sample was rotated such that the ball slid across the sample surface in a circular motion with a radius of 1.2 mm and at a linear speed of 1.0 cm s^{-1}. Each test was carried out on at least two locations on each sample for up to 10 000 cycles while the coefficient of friction, μ, was measured. After the test, the wear track and ball images were captured by using an optical microscope.

During the surface modification process, the C^+ ions may also interact with the magnetic recording media. Hence, it is crucial to investigate any change in the macromagnetic properties of the magnetic media. The macromagnetic properties of the disk samples after surface modification were measured using a custom-made magneto-optic Kerr effect (MOKE) setup to investigate whether the surface modification process had significantly affected the magnetic performance of the magnetic media. The hysteresis loops of Kerr rotation with respect to the applied magnetic field for samples 16C, 4SiN12C, and CM were recorded and compared.

At ultralow thicknesses, protection of the underlying hard disk media from corrosion or oxidation becomes critical to prevent the degradation of the magnetic material over time which would lead to the loss of stored data. To understand the effectiveness of the overcoats in protecting the underlying media from corrosion, a custom-made three-electrode corrosion setup was used to perform

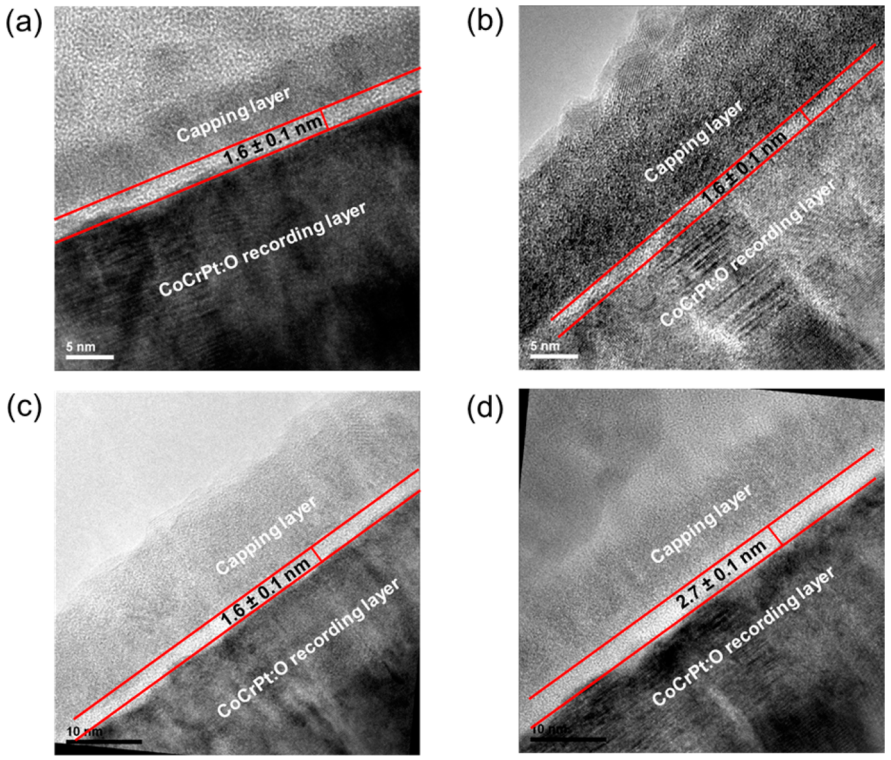

Figure 3. Cross-sectional TEM images showing the thickness of the overcoats (labeled in red) for samples (a) 16C, (b) 16SiN, (c) 4SiN12C, and (d) CM.

electrochemical potentiodynamic polarization measurements on all the samples.[18] An electrolyte solution of 0.1 M NaCl was used during the test, and a geometric surface area of 0.24 cm^2 of the sample surface was exposed to the electrolyte. Each electrochemical test consisted of an anodic sweep and a cathodic sweep where the potential was varied and the corresponding current was measured. In the anodic sweep, the potential was swept 0.4 V above the open circuit potential, whereas in the cathodic sweep the potential was swept 0.4 V below the open circuit potential. Every sweep was conducted at a different location on the sample, with at least three sets of tests (6 sweeps) conducted on each sample to obtain consistent readings. The test best representing the consistent result is presented.

X-ray photoelectron spectroscopy (XPS) was used to characterize the chemical bonding and oxidation resistance performance of the carbon-containing overcoats, namely, 16C, 4SiN12C, and CM. XPS measurements were performed using a VG ESCALAB 220I-XL spectrometer with an Al Kα source. The microstructures of the carbon overcoats in these samples were probed with visible and UV Raman spectroscopy (Jobin Yvon LABRAM-HR) at laser excitation wavelengths of 488 and 325 nm, respectively. To avoid damage to ultrathin COCs due to the laser heating of the sample surface, the laser power was kept low and other parameters such as the charge coupled device's (CCD) exposure and data acquisition time were synchronized to obtain a reasonable signal-to-noise ratio for all samples. The relative intensity ratios of the COCs were compared from various locations of the sample surfaces to distinguish the nature of the carbon bonding with an accuracy of <2%. Here, we briefly discuss the XPS and Raman data to correlate the microstructural properties with the functional performance of the overcoats based on the tribological and corrosion results. More detailed XPS and Raman analyses of these overcoats can be found in one of our recent studies.[26]

3. RESULTS AND DISCUSSION

The cross-sectional TEM images of samples 16C, 16SiN, 4SiN12C, and CM are presented in Figure 3. From the images, the thicknesses of the overcoats in samples 16C, 16SiN, and 4SiN12C were each measured to be ~1.6 ± 0.1 nm, while the thickness of the COC in sample CM was measured to be 2.7 ± 0.1 nm. It is evident that the deposited overcoat thicknesses in samples 16C, 16SiN, and 4SiN12C matched well with our calibration, revealing that our process can be precisely controlled even at ultrathin levels. In sample 4SiN12C, however, owing to the extremely low thickness of the SiN_x layer and similar contrast to carbon, it is difficult to distinguish it from the FCVA-deposited carbon layer. Consequently, only the total overcoat thickness of ~1.6 ± 0.1 nm was measured. The presence of SiN_x in sample 4SiN12C was subsequently confirmed by XPS analysis, which will be discussed later.

The average roughness (R_a) and root-mean-square roughness (R_q) of the four samples were measured, as shown in Figure 4. It can be seen that the R_q of the COC in commercial disks

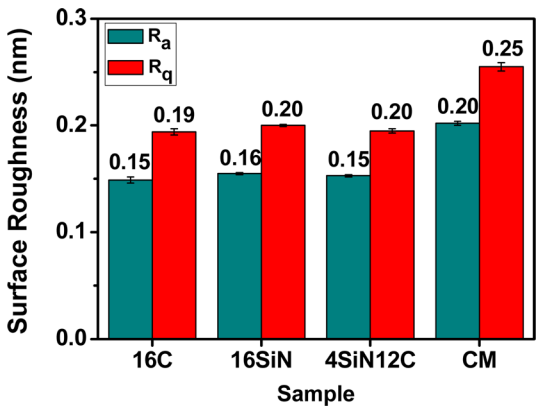

Figure 4. Average roughness (R_a) and root-mean-square roughness (R_q) values of samples 16C, 16SiN, 4SiN12C, and CM.

dx.doi.org/10.1021/am501760p | ACS Appl. Mater. Interfaces 2014, 6, 9376−9385

(sample CM) is ~0.25 nm. Surprisingly, the disks which had undergone the surface modification process of overcoat deposition by FCVA carbon exhibited at least 20% lower R_q compared to the commercial disk sample, with values between ~0.19 to ~0.20 nm. It is proposed that the decrease in the surface roughness could be contributed by the surface etching process before overcoat deposition, which may have smoothened the surface of the underlying rough magnetic media. To a certain extent, the FCVA process may have also contributed to the improvement in surface smoothness.[7] A low surface roughness is a desirable feature for better tribological and corrosion performances, and at the nanoscale regime it is beneficial for reducing the magnetic spacing for higher storage densities.

The frictional curves (μ versus number of cycles) measured during the tribological tests are shown in Figure 5a, and the variation of μ for different samples is shown in Figure 5b. The optical images of the counterface ball and the wear track region are shown in Figure 6a–e and f–j, respectively. It is evident that, without any protective overcoat, sample BM exhibits the highest $\mu \sim 0.70 \pm 0.10$ over the whole duration of the test with large fluctuations. The bare media has soft magnetic layers, which are easily worn upon sliding with the counterface balls. The excessive wear in sample BM can be seen in optical images as shown in Figure 6e and j. Sample 16SiN gives a μ value of between 0.55 ± 0.05, which is characteristic of monolithic SiN_x as shown elsewhere by Rismani et al.[27] We have also observed severe wear tracks and debris on the sample surfaces and counterface ball, respectively. Thus, it can be seen that the tribological performance of the monolithic SiN_x layer is poor. On the other hand, the μ of the commercial disk COC in sample CM was found to be ~0.35 and showed large fluctuation throughout the test. The optical images of sample CM (Figure 6d and i) also showed considerable amount of material transfer to the ball and severe wear track, indicating the poor wear resistance of commercial COC. What is interesting here is that samples 16C and 4SiN12C, which have FCVA-deposited COCs, exhibited μ values lower than that of CM which contains commercially grown COC. While sample 16C showed lower $\mu \sim 0.25 \pm 0.03$, negligible material transfer to the counterface ball and a very faint wear track, the best tribological performance was observed for sample 4SiN12C with the SiN_x/C bilayer overcoat. Sample 4SiN12C exhibited a μ value of $\sim 0.18 \pm 0.02$ which was found to be very stable until the end of test, along with a negligible amount of material transfer to the ball and no visible wear track. These results highlight the efficacy of FCVA-deposited carbon in acting as an excellent wear-resistant layer with low friction, and the improvement in the frictional properties conveys the benefit of the addition of an atomically thin SiN_x underlayer. The improved tribological characteristics provided by the SiN_x/C bilayer overcoat can be attributed to the increased interfacial bonding and enhanced sp^3 carbon hybridization.

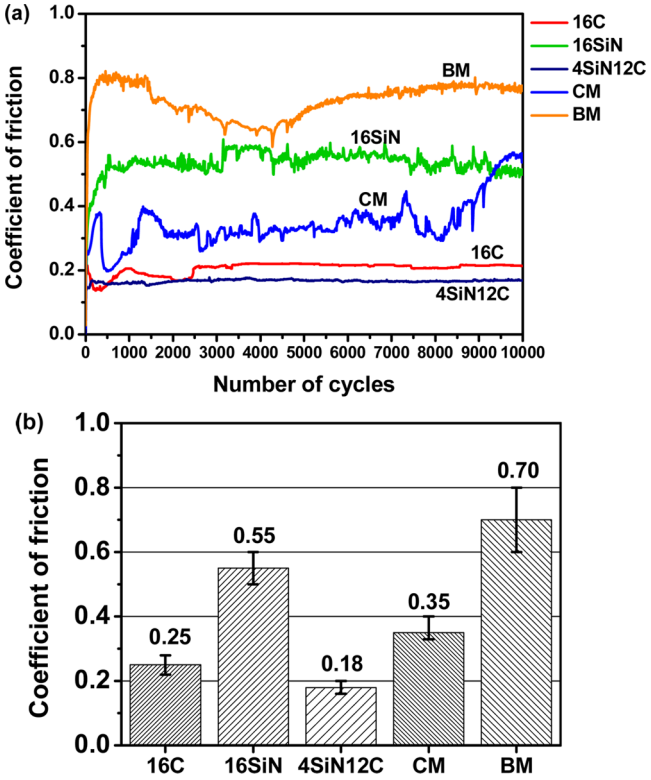

Figure 5. (a) Summary of coefficient of friction data with respect to number of cycles as obtained from ball-on-disk tribological tests; (b) bar chart showing the average coefficient of friction values for each sample.

The macromagnetic properties of the hard disk can be characterized based on its magnetization behavior under an applied switching magnetic field. In this work, the magnetization behavior is measured by MOKE, where the Kerr rotation, which is directly related to the sample magnetization, is detected under a changing magnetic field. The magnetization hysteresis loops of samples 16C, 16SiN, 4SiN12C, and CM obtained from the MOKE measurements are shown in Figure 7. It is apparent that the hysteresis loops for samples 16C, 16SiN, and 4SiN12C are almost identical and overlap with each other. As compared to the as-received commercial disk sample CM, the macromagnetic properties such as the coercivity and

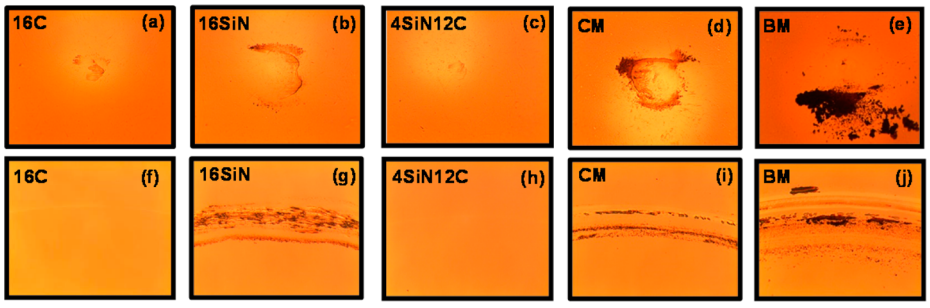

Figure 6. Optical images of (a–e) counterface ball and (f–j) samples after the ball-on-disk tribological tests.

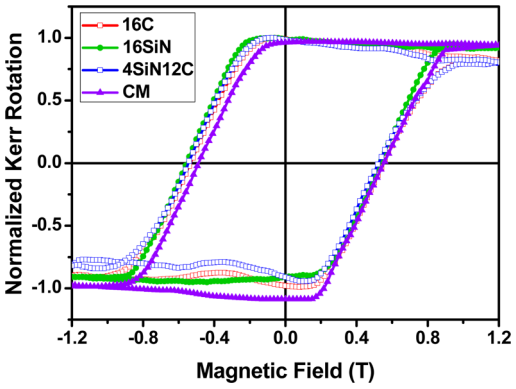

Figure 7. MOKE hysteresis loops of samples 16C, 16SiN, 4SiN12C, and CM under an applied switching magnetic field.

switching field distribution show little difference. This shows that the surface modification and overcoat deposition process did not significantly affect the macromagnetic properties of the magnetic media.

One of the motivations for using the bilayer structure with a SiN_x underlayer, as mentioned earlier, is to provide a chemically inert diffusion barrier layer which hinders the diffusion of small molecules and ions into the magnetic media.[20] In doing so, the rate of oxidation and corrosion of the magnetic media could possibly be reduced. After potentiodynamic polarization tests were conducted on the samples, the measured potential and current data were extracted from the anodic and cathodic sweeps and plotted on a semilogarithmic plot of potential versus current density, as shown in Figure 8. The corrosion

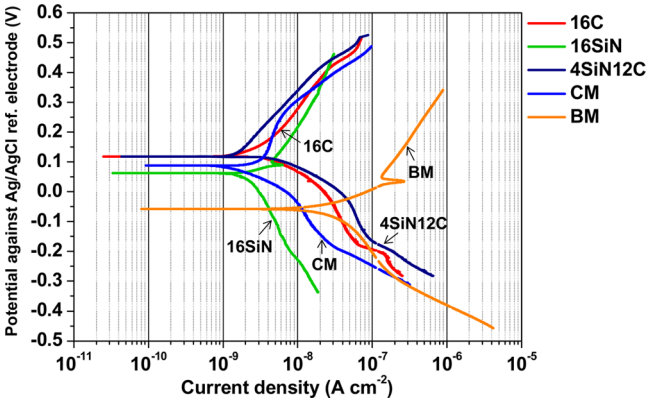

Figure 8. Potentiodynamic polarization curves of samples 16C, 16SiN, 4SiN12C, CM, and BM measured by our custom-made three-electrode electrochemical setup.

performance of the samples can be compared by a method known as Tafel extrapolation, where the linear portions of the anodic and cathodic curves are extrapolated toward the open circuit potential.[28] The intersection of the extrapolations at a certain current density would indicate the corrosion current density (j_{corr}), which is a measure of the propensity of the sample to undergo corrosion. Hence, the j_{corr} is inversely proportional to the corrosion resistance of the sample, that is, the higher the j_{corr} value, the lower the corrosion resistance of the sample.

Figure 9 summarizes the j_{corr} values extracted from the curves in Figure 8. Not surprisingly, for bare magnetic media without COC, the average j_{corr} is the highest at 15×10^{-9} A cm^{-2}. On

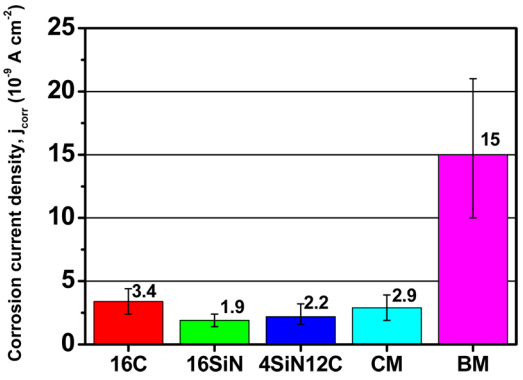

Figure 9. Corrosion current density (j_{corr}) values of tested disk samples extracted from Figure 8.

the other hand, the average j_{corr} of sample 16SiN is the lowest among the four samples which shows that monolithic SiN_x acts as a good corrosion protection barrier. When comparing sample 4SiN12C with sample 16C, sample 4SiN12C has a lower average j_{corr}. This can be attributed to the additional corrosion protection provided by the SiN_x underlayer, as well as the generation of a higher sp^3 carbon bonding fraction which improves the density of the carbon overcoat layer in sample 4SiN12C (which will be discussed later). Furthermore, although samples 16C, 16SiN, and 4SiN12C have ~40% lower overcoat thickness compared to sample CM, it can be seen that the corrosion resistance has not been adversely affected. This shows that the single layer FCVA-deposited COC, single layer SiN_x overcoat and the SiN_x/C bilayer overcoat still provide good corrosion protection of the media at thicknesses of <2 nm.

The corrosion performance can be succinctly summarized and compared using the concept of protective efficiency (PE), which gives a measure of the overcoat's corrosion protection capability with respect to bare magnetic media. The formula for the PE of the overcoat is given by

$$\%\mathrm{PE} = \frac{j_{corr}^{0} - j_{corr}}{j_{corr}} \times 100$$

where j_{corr}^{0} is the value of the extrapolated corrosion current density of bare magnetic media (sample BM).[18,29] The calculated PEs of the tested samples are summarized in Table 2. Based on the results shown in Table 2 and taking the

Table 2. Summary of the Protective Efficiencies of the different overcoats

sample	overcoat structure	PE (%)
16C	C (16 Å)	77.3
16SiN	SiN_x (16 Å)	87.3
4SiN12C	SiN_x (4 Å)|C (12 Å)	85.3
CM	commercial COC (~27 Å)	80.7
BM	no COC	0.0

tribological results into account, the SiN_x/C bilayer overcoat used in sample 4SiN12C is found to be the best protective overcoat material.

To investigate the chemical structure and oxidation within the carbon-containing overcoats, XPS measurements were performed at a photoelectron takeoff angle of 65° with respect to the analyzed surface. Background correction was performed

dx.doi.org/10.1021/am501760p | ACS Appl. Mater. Interfaces 2014, 6, 9376−9385

before fitting the XPS core level spectra of each element to remove any background noise. Figure 10a–c shows the C 1s

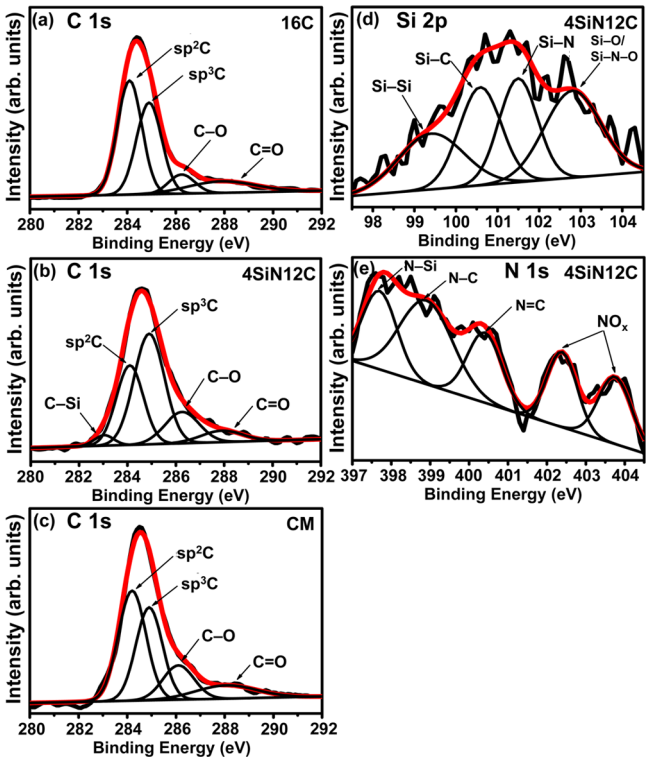

Figure 10. Deconvoluted C 1s core level XPS spectra of samples (a) 16C, (b) 4SiN12C, and (c) CM. Deconvoluted (d) Si 2p and (e) N 1s core level spectra of sample 4SiN12C.

core level spectra of samples 16C, 4SiN12C, and CM. The fitting of the C 1s core level spectra was performed with a Gaussian curve, where all the samples exhibited four constituent peaks corresponding to the sp^2 bonding in carbon (sp^2C, at 284.1 ± 0.1 eV), sp^3 bonding in carbon (sp^3C, at 284.9 eV), C–O bonding (at 286.2 ± 0.1 eV), and C=O bonding (at 287.9 ± 0.1 eV).[9,15,30,31] An additional peak at ~283.0 eV was observed only in sample 4SiN12C, which is assigned to C–Si bonding.[15,24] The formation of C–Si bonding can be attributed to the interaction of C^+ ions with the SiN_x underlayer at the SiN_x/C interface. To further confirm the interfacial bonding of C with Si and C with N, the Si 2p and N 1s core level spectra of sample 4SiN12C were also fitted with various Gaussian components, as shown in Figure 10d and e. The four constituent peaks observed in the Si 2p core level spectrum are assigned to Si–Si bonding (at 99.4 eV), Si–C bonding (at 100.6 eV), Si–N bonding (at 101.5 eV), and Si–O/Si–N–O bonding (at 102.8 eV). Similarly, five constituent peaks found in the N 1s core level spectrum are assigned to N–Si bonding (at 397.7 eV), N-sp^3C bonding (at 398.9 eV), N-sp^2C bonding (at 400.4 eV), and N–O_x bonding (at 402.4 and 403.7 eV).[32–34]

After analyzing the Si 2p, N 1s, and C 1s core level spectra, the Co $2p_{3/2}$ core level spectra of the magnetic media for samples 16C, 4SiN12C, and CM were also examined. As shown in Figure 11a–c, the Co $2p_{3/2}$ spectra for all three samples were fitted with various Gaussian–Lorentzian components. The peaks observed in each Co $2p_{3/2}$ core level spectrum can be assigned to Co–Co bonding (at 778.0 ± 0.1 eV), Co oxide bonding in Co_2O_3 (at 779.2 ± 0.1 eV), cobalt oxide/hydroxide

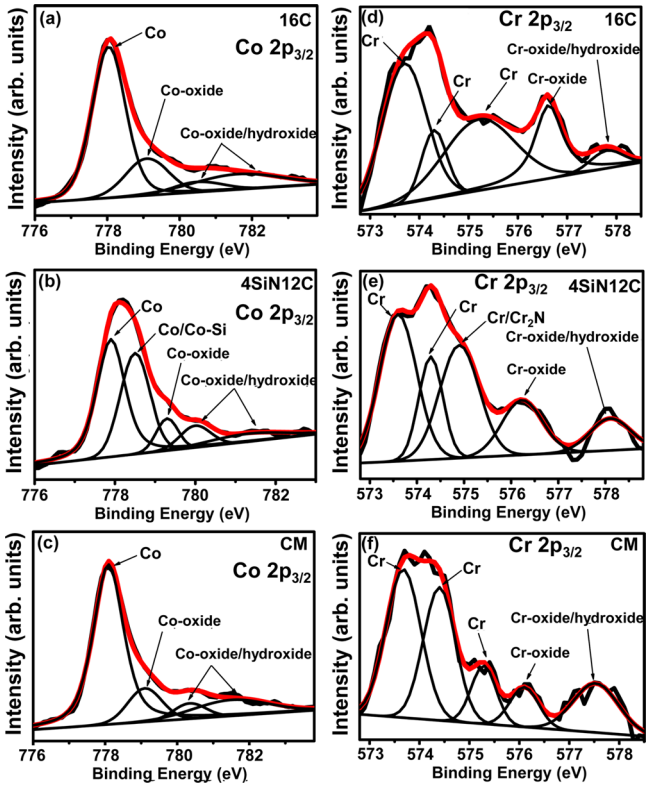

Figure 11. Deconvoluted Co $2p_{3/2}$ core level XPS spectra of samples (a) 16C, (b) 4SiN12C, and (c) CM. Deconvoluted Cr $2p_{3/2}$ core level XPS spectra of samples (d) 16C, (e) 4SiN12C, and (f) CM.

bonding in CoO, Co_3O_4, CoOOH or $Co(OH)_2$ (at 780.3 ± 0.3 eV), and cobalt oxide/hydroxide bonding in CoO, Co_3O_4, or $Co(OH)_2$ (at 781.5 ± 0.2 eV).[15,35–37] In addition, a fifth peak at 778.5 eV corresponding to Co–Si bonding was observed only in sample 4SiN12C, attributed to the interfacial bonding between Si in the SiN_x layer and Co in the magnetic recording media.[15,38] It should be noted that this peak may also be influenced by metallic Co bonding. Similarly, the Cr $2p_{3/2}$ core level spectra were also analyzed and fitted with various Gaussian–Lorentzian components, and are shown in Figure 11d–f. The deconvoluted peaks as shown in the Cr $2p_{3/2}$ core level spectra can be assigned to Cr–Cr (at 573.7 ± 0.1 eV and 574.3 ± 0.1 eV), Cr–oxide (at 576.2 ± 0.4 eV), and Cr–oxide/hydroxide (at 577.8 ± 0.3 eV) bonding, respectively.[35,37,39,40] Extra care was taken to analyze the peaks located at 575.2 ± 0.1 and 574.9 eV. For samples 16C and CM, the peak observed at 575.2 ± 0.1 eV is ascribed to Cr–Cr bonding, whereas in sample 4SiN12C the peak observed at 574.9 eV may also have some contribution from Cr_2N bonding at the interface in addition to the Cr–Cr bonding thus explaining the slight shift in the binding energy.[41] It is important to note that the reason for fitting more than one peak to Cr–Cr bonding was only to get the best fit to the data.

The constituent peaks in all the core level spectra obtained for all the samples were quantitatively analyzed using an area ratio method, which compares the areas under the constituent peaks. The bonding fractions are summarized in Table 3. From the XPS analyses, it is evident that the introduction of the 4 Å SiN_x underlayer causes a significant change in the microstructure of the carbon film by creating higher amounts of interfacial bonding between the carbon and SiN_x layer, increasing the sp^3C bonding fraction, and reducing the amount

dx.doi.org/10.1021/am501760p | ACS Appl. Mater. Interfaces 2014, 6, 9376–9385

Table 3. Quantitative Measure of Bonding Fractions in Samples 16C, 4SiN12C, and CM Using an Area Ratio Method

	bonding fractions				
sample	sp^3C	Co−Co/Co−Si	Co−oxide/Co−hydroxide	Cr−Cr/Cr_2N	Cr−oxide/Co−hydroxide
16C	∼37%	∼62%	∼38%	∼79%	∼21%
4SiN12C	∼46%	∼78%	∼22%	∼79%	∼21%
CM	∼33%	∼68%	∼32%	∼76%	∼24%

of oxidation of the underlying magnetic media. When comparing the sp^3C bonding fraction of FCVA-deposited carbon films with and without the SiN_x underlayer (i.e., samples 16C and 4SiN12C, respectively), while keeping total coating thickness constant at 16 Å, sample 4SiN12C shows higher sp^3C bonding with an absolute difference of ∼9% as compared to sample 16C (corresponding to an ∼25% increase in relative terms). When compared with the commercial COC in sample CM, the FCVA-deposited carbon in the SiN_x/C bilayer overcoat of sample 4SiN12C shows ∼13% higher sp^3C bonding in absolute terms (corresponding to a relative increase of ∼40%), despite an ∼40% reduction in the total overcoat thickness. This difference is quite significant, especially at the ultrathin film level. The enhanced sp^3C bonding in the SiN_x/C bilayer overcoat helps to improve oxidation protection of the underlying media, which is reflected by the reduction in the oxidation level of the Co and Cr. Still, even without a SiN_x underlayer, the monolithic FCVA-deposited COC in sample 16C exhibited better oxidation protection than a thicker commercial COC in sample CM.

The introduction of the SiN_x underlayer between the media and COC in the SiN_x/C bilayer overcoat gives rise to two advantageous effects. First, it enhances the adhesion between the COC and media by promoting the interfacial bonding. XPS analysis shows the formation of strong interfacial bonds at the SiN_x/C and SiN_x/media interfaces (such as Co−Si, Cr_2N, Si−C, and C−N). This suggests that it is a good adhesion layer. At the same time, the SiN_x underlayer functions as a barrier between the media and COC and helps in enhancing the sp^3C bonding fraction. The enhancement of the sp^3C fraction can be explained based on the interaction of the arriving energetic C^+ ions with the magnetic media substrate, with and without the SiN_x layer. When the carbon film is grown directly onto the magnetic media (like in sample 16C), the Co and Pt atoms present in the media promotes sp^2 carbon bonding at the media−carbon interface due to a catalytic effect.[42,43] However, when an ultrathin layer of SiN_x is introduced over the media, it acts as a barrier between the media and the arriving C^+ ions, which reduces this catalytic reaction to some extent. The interaction of the C^+ ions with Si and N in the SiN_x layer also reduces the probability of carbon interaction with Co and Pt in the media. The suppression of the catalytic reaction to some extent helps in enhancing the sp^3C bonding. Hence, the combined usefulness of the SiN_x underlayer as both an adhesion layer and barrier layer has led to the improved corrosion/oxidation resistance and better tribological properties in terms of low COF and high wear resistance in the SiN_x/C bilayer overcoat.

Visible and UV Raman spectroscopy measurements were performed to gain further insight into the microstructures of the carbon-containing overcoats. The visible Raman spectra for samples 16C, 4SiN12C, and CM are shown in Figure 12a−c, while their UV Raman spectra are shown in Figure 12d−f. The visible Raman spectra of these samples each show two characteristic peaks corresponding to the disorder (D) peak

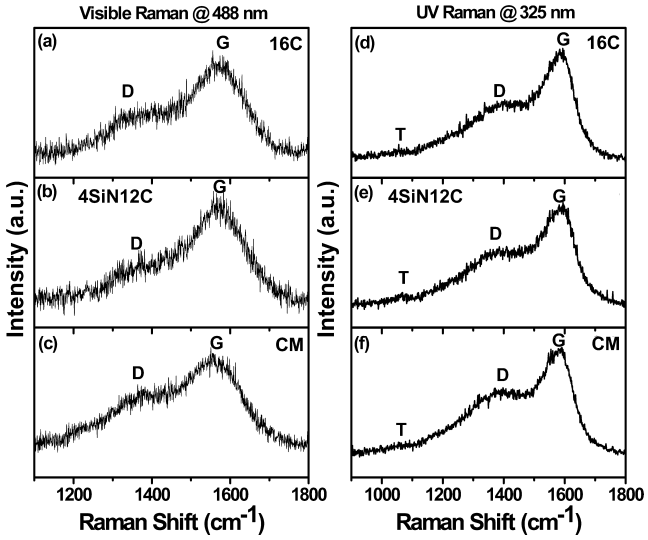

Figure 12. Visible Raman spectra for samples (a) 16C, (b) 4SiN12C, and (c) CM. UV Raman spectra for samples (d) 16C, (e) 4SiN12C, and (f) CM.

centered in the wavenumber range of 1380−1405 cm^{-1} and the G peak centered in the range of 1565−1580 cm^{-1}. The D peak is contributed by the breathing mode of sp^2C atoms in aromatic rings, whereas the G peak arises from the in-plane bond stretching motion of all pairs of sp^2C atoms in both rings and chains.[44] Hence, the D and G peaks are both associated with sp^2C bonding. UV Raman spectroscopy was conducted using higher energy photons than visible Raman so as to probe the vibrational mode of sp^3-bonded carbon, which cannot be observed using visible excitation wavelengths. In addition to its characteristic D and G peaks, the UV Raman spectra of the three samples showed an additional peak centered in the range of 1050−1100 cm^{-1}, albeit weak. This peak is known as the T peak. Ferrari and Robertson have made similar observations of such a low intensity T peak in FCVA-deposited carbon films with 325 nm UV excitation.[44−46] The T peak corresponds to the vibration of the sp^3C bonds in amorphous carbon films. It should be noted that the T peak has a slightly higher intensity in sample 4SiN12C than in samples 16C and CM. This indicates that sample 4SiN12C has relatively higher sp^3C bonding than the other two samples. This finding agrees well with our XPS analysis.

While the G peak is associated with sp^2C bonding, the relative shifts in the G peak position can be used to probe changes in sp^3C and sp^2C bonding under UV excitation. On the other hand, visible Raman spectroscopy can be employed to explain the nature of sp^2 carbon clustering in different samples due to its predominant sensitivity to sp^2C bonding. The visible and UV Raman spectra of the samples were fitted with two Gaussian components, and their exact D and G peak positions and the ratios of the D-to-G peak intensities (I_D/I_G ratios) were determined. The G peak positions in the UV Raman spectra of

samples 16C, 4SiN12C, and CM were found to be 1586, 1588, and 1582.0 cm^{-1}, respectively. According to the three-stage model proposed by Ferrari and Robertson,[44] the shift in the G peak position toward higher wavenumbers during the third stage implies an increase in the sp^3C bonding fraction. Since the XPS results reveal the trend of the sp^3C bonding fraction to be 4SiN12C > 16C > CM, our Raman results corroborate well with the XPS analysis. Furthermore, the I_D/I_G ratios (at excitation wavelength of 488 nm) in samples 16C, 4SiN12C, and CM were found to be 0.5, 0.4, and 0.6, respectively. This indicates that sample 4SiN12C inhibits the development of sp^2 carbon clusters as compared to other samples. Hence, as interpreted from the Raman and XPS spectra, it can be seen that the introduction of a 4 Å thick SiN_x underlayer between the media and an FCVA-deposited COC helps to increase the sp^3 carbon bonding and lower the sp^2 carbon clustering within the COC.

4. CONCLUSIONS

A bilayer of reactively sputtered 4 Å of SiN_x followed by 12 Å of FCVA-deposited carbon (SiN_x/C) has been explored as a proposed overcoat structure for high storage density application. SiN_x has been known and reported to have good corrosion protection down to thicknesses of 1 nm,[47] but on its own it does not exhibit good tribological properties. On the other hand, FCVA-deposited carbon at suitably optimized energies is known to possess good tribological properties. In this work, the development of the SiN_x/C bilayer structure, aimed to enrich the sp^3C content to obtain the benefits of good corrosion/oxidation protection with good tribological properties at ultralow thicknesses of <2 nm, is demonstrated.

The key finding from this work is that when an atomically thin interfacial SiN_x layer is applied between CoCrPt:Oxide based media and a FCVA-deposited COC, its advantage is threefold. First, it acts as an adhesion layer due to increased interfacial bonding, which improves the adhesion between the magnetic media and the COC. Second, due to the dense structure and chemical inertness of SiN_x, it acts as a barrier layer to hinder the diffusion of metallic ions and small molecules (such as water and oxygen) through the overcoat and reduces corrosion and oxidation in the media. Third, it suppresses the catalytic reaction of Co and Pt in the media with the incoming energetic C^+ ions. The suppression of the catalytic effect helps to increase the sp^3 carbon fraction in the carbon layer of the bilayer overcoat by ∼40% when compared to conventionally deposited COC in today's commercial magnetic disks (change from ∼33% sp^3C in conventional COC to ∼46% sp^3C in the 16 Å SiN_x/C bilayer overcoat), and by ∼25% when compared to monolithic 16 Å FCVA-deposited COC (change from ∼37% sp^3C in 16 Å FCVA-deposited COC to ∼46% sp^3C in the 16 Å SiN_x/C bilayer overcoat). This is even more remarkable given that the bilayer overcoat has ∼40% lower thickness than commercial disk COC. With reduced diffusion through the overcoat, higher sp^3 carbon content and improved interfacial bonding, it is seen that the SiN_x/C bilayer overcoat was able to provide a low and stable COF as well as better wear and corrosion/oxidation protection of the magnetic media. This was confirmed by ball-on-disk tribological tests, XPS, and electrochemical corrosion measurements. It was also observed that the etching and deposition process during fabrication of the monolithic and bilayer overcoats did not cause surface roughening or degrade the macromagnetic properties of the magnetic media.

In summary, the fabrication of our proposed SiN_x/C bilayer overcoat structure by surface modification of commercial hard disks has demonstrated enhanced sp^3 carbon content at ultrathin overcoat thickness (<2 nm) with desirable corrosion and tribological performance, without degrading the magnetic properties. With the high sp^3 carbon content and low thickness of the SiN_x/C overcoat, it is a promising candidate for providing low magnetic spacing and high thermal stability, which are critical factors for high density storage and HAMR application in future HDDs.

AUTHOR INFORMATION

Corresponding Author

*E-mail: elebcs@nus.edu.sg.

Notes

The authors declare no competing financial interest.

ACKNOWLEDGMENTS

This research is supported by the National Research Foundation, Prime Minister's Office, Singapore under its Competitive Research Programme (CRP Award No. NRF-CRP 4-2008-06).

REFERENCES

(1) Wallace, R. L. The Reproduction of Magnetically Recorded Signals. *Bell Syst. Tech. J.* **1951**, *30*, 1145−1173.
(2) Bandic, Z. Z.; Victora, R. H. Advances in Magnetic Data Storage Technologies. *Proc. IEEE* **2008**, *96*, 1749−1753.
(3) Yuan, Z. M.; Liu, B.; Zhou, T. J.; Goh, C. K.; Ong, C. L.; Cheong, C. M.; Wang, L. Perspectives of Magnetic Recording System at 10 Tb/in(2). *IEEE Trans. Magn.* **2009**, *45*, 5038−5043.
(4) Marchon, B.; Pitchford, T.; Hsia, Y.-T.; Gangopadhyay, S. The Head-Disk Interface Roadmap to an Areal Density of 4 Tbit/in^2. *Adv. Tribol.* **2013**, *2013*, 1−8.
(5) Rose, F.; Marchon, B.; Rawat, V.; Pocker, D.; Xiao, Q.-F.; Iwasaki, T. Ultrathin TiSiN Overcoat Protection Layer for Magnetic Media. *J. Vac. Sci. Technol., A* **2011**, *29*, 051502.
(6) Kryder, M. H.; Gage, E. C.; McDaniel, T. W.; Challener, W. A.; Rottmayer, R. E.; Ju, G.; Hsia, Y.-T.; Erden, M. F. Heat Assisted Magnetic Recording. *Proc. IEEE* **2008**, *96*, 1810−1835.
(7) Bhatia, C. S.; Anders, S.; Bobb, K.; Hsiao, R.; Brown, I. G.; Bogy, D. B. Ultra-Thin Overcoats for the Head/Disk Interface Tribology. *J. Tribol.* **1998**, *120*, 795−799.
(8) Casiraghi, C.; Ferrari, A. C.; Ohr, R.; Chu, D.; Robertson, J. Surface Properties of Ultra-Thin Tetrahedral Amorphous Carbon Films for Magnetic Storage Technology. *Diamond Relat. Mater.* **2004**, *13*, 1416−1421.
(9) Robertson, J. Requirements of Ultrathin Carbon Coatings for Magnetic Storage Technology. *Tribol. Int.* **2003**, *36*, 405−415.
(10) Zhang, H. S.; Komvopoulos, K. Surface Modification of Magnetic Recording Media by Filtered Cathodic Vacuum Arc. *J. Appl. Phys.* **2009**, *106*, 093504.
(11) Xu, S.; Flynn, D.; Tay, B. K.; Prawer, S.; Nugent, K. W.; Silva, S. R. P.; Lifshitz, Y.; Milne, W. I. Mechanical Properties and Raman Spectra of Tetrahedral Amorphous Carbon Films with High sp^3 Fraction Deposited Using a Filtered Cathodic Arc. *Philos. Mag. B* **1997**, *76*, 351−361.
(12) Parthem, B. K.; Guo, X.-C.; Rose, F.; Wang, N.; Komvopoulos, K.; Schreck, E.; Marchon, B. Carbon Overcoat Oxidation in Heat-Assisted Magnetic Recording. *IEEE Trans. Magn.* **2013**, *49*, 3721−3724.
(13) Jones, P. M.; Ahner, J.; Platt, C. L.; Tang, H.; Hohlfeld, J. Understanding Disk Carbon Loss Kinetics for Heat Assisted Magnetic Recording. *IEEE Trans. Magn.* **2014**, *50*, 3300704.
(14) Pharr, G. M.; Callahan, D. L.; McAdams, S. D.; Tsui, T. Y.; Anders, S.; Anders, A.; Ager, J. W.; Brown, I. G.; Bhatia, C. S.; Silva, S.

R. P.; Robertson, J. Hardness, Elastic Modulus, and Structure of Very Hard Carbon Films Produced by Cathodic-Arc Deposition with Substrate Pulse Biasing. *Appl. Phys. Lett.* **1996**, *68*, 779−781.
(15) Ferrari, A. C. Diamond-Like Carbon for Magnetic Storage Disks. *Surf. Coat. Technol.* **2004**, *180−181*, 190−206.
(16) Samad, M. A.; Rismani, E.; Yang, H.; Sinha, S. K.; Bhatia, C. S. Overcoat Free Magnetic Media for Lower Magnetic Spacing and Improved Tribological Properties for Higher Areal Densities. *Tribol. Lett.* **2011**, *43*, 247−256.
(17) Samad, M. A.; Xiong, S. M.; Pan, L.; Yang, H.; Sinha, S. K.; Bogy, D. B.; Bhatia, C. S. A Novel Approach of Carbon Embedding in Magnetic Media for Future Head/Disk Interface. *IEEE Trans. Magn.* **2012**, *48*, 1807−1812.
(18) Yeo, R. J.; Rismani, E.; Dwivedi, N.; Blackwood, D. J.; Tan, H. R.; Zhang, Z.; Tripathy, S.; Bhatia, C. S. Bi-Level Surface Modification of Hard Disk Media by Carbon Using Filtered Cathodic Vacuum Arc: Reduced Overcoat Thickness Without Reduced Corrosion Performance. *Diamond Relat. Mater.* **2014**, *44*, 100−108.
(19) Rismani, E.; Samad, M. A.; Sinha, S. K.; Yeo, R.; Yang, H.; Bhatia, C. S. Ultrathin Si/C Graded Layer to Improve Tribological Properties of Co Magnetic Films. *Appl. Phys. Lett.* **2012**, *101*, 191601.
(20) Yen, B. K.; White, R. L.; Waltman, R. J.; Dai, Q.; Miller, D. C.; Kellock, A. J.; Marchon, B.; Kasai, P. H.; Toney, M. F.; York, B. R.; Deng, H.; Xiao, Q. F.; Raman, V. Microstructure and Properties of Ultrathin Amorphous Silicon Nitride Protective Coating. *J. Vac. Sci. Technol., A* **2003**, *21*, 1895−1904.
(21) Azzi, M.; Amirault, P.; Paquette, M.; Klemberg-Sapieha, J. E.; Martinu, L. Corrosion Performance and Mechanical Stability of 316L/DLC Coating System: Role of Interlayers. *Surf. Coat. Technol.* **2010**, *204*, 3986−3994.
(22) Chiang, J. N.; Ghanayem, S. G.; Hess, D. W. Low-Temperature Hydrolysis (Oxidation) of Plasma-Deposited Silicon Nitride Films. *Chem. Mater.* **1989**, *1*, 194−198.
(23) Singhal, S. C. Thermodynamics and Kinetics of Oxidation of Hot-Pressed Silicon Nitride. *J. Mater. Sci.* **1976**, *11*, 500−509.
(24) Bunnak, P.; Gong, Y.; Limsuwan, S.; Pokaipisit, A.; Limsuwan, P. Chemical Bonding in Composite SiN_x/Diamond-Like Carbon Films Prepared by Filter Cathodic Arc Deposition of Graphite Incorporated with Radio Frequency Sputtering of Silicon Nitride. *Jpn. J. Appl. Phys.* **2013**, *52*, 095501.
(25) Chhowalla, M.; Robertson, J.; Chen, C. W.; Silva, S. R. P.; Davis, C. A.; Amaratunga, G. A. J.; Milne, W. I. Influence of Ion Energy and Substrate Temperature on the Optical and Electronic Properties of Tetrahedral Amorphous Carbon (ta-C) Films. *J. Appl. Phys.* **1997**, *81*, 139−145.
(26) Dwivedi, N.; Rismani-Yazdi, E.; Yeo, R. J.; Goohpattader, P. S.; Satyanarayana, N.; Srinivasan, N.; Druz, B.; Tripathy, S.; Bhatia, C. S. Probing the Role of an Atomically Thin SiN_x Interlayer on the Structure of Ultrathin Carbon Films. *Sci. Rep.* **2014**, *4*, 5021.
(27) Rismani, E.; Yeo, R.; Mirabolghasemi, H.; Kwek, W. M.; Yang, H.; Bhatia, C. S. An Ultrathin Multilayer TiN/SiN Wear Resistant Coating for Advanced Magnetic Tape Drive Heads. *Thin Solid Films* **2014**, *556*, 354−360.
(28) Hoar, T. P. On the Relation Between Corrosion Rate and Polarization Resistance. *Corros. Sci.* **1967**, *7*, 455−458.
(29) Khun, N. W.; Liu, E.; Krishna, M. D. Structure, Adhesive Strength and Electrochemical Performance of Nitrogen Doped Diamond-Like Carbon Thin Films Deposited via DC Magnetron Sputtering. *J. Nanosci. Nanotechnol.* **2010**, *10*, 4752−4757.
(30) Wang, N.; Komvopoulos, K. Incidence Angle Effect of Energetic Carbon Ions on Deposition Rate, Topography, and Structure of Ultrathin Amorphous Carbon Films Deposited by Filtered Cathodic Vacuum Arc. *IEEE Trans. Magn.* **2012**, *48*, 2220−2227.
(31) Zhang, H.-S.; Komvopoulos, K. Synthesis of Ultrathin Carbon Films by Direct Current Filtered Cathodic Vacuum Arc. *J. Appl. Phys.* **2009**, *105*, 083305.
(32) Matsuoka, M.; Isotani, S.; Sucasaire, W.; Zambom, L. S.; Ogata, K. Chemical Bonding and Composition of Silicon Nitride Films Prepared by Inductively Coupled Plasma Chemical Vapor Deposition. *Surf. Coat. Technol.* **2010**, *204*, 2923−2927.
(33) McCann, R.; Roy, S. S.; Papakonstantinou, P.; Bain, M. F.; Gamble, H. S.; McLaughlin, J. A. Chemical Bonding Modifications of Tetrahedral Amorphous Carbon and Nitrogenated Tetrahedral Amorphous Carbon Films Induced by Rapid Thermal Annealing. *Thin Solid Films* **2005**, *482*, 34−40.
(34) Yan, X. B.; Xu, T.; Chen, G.; Yang, S. R.; Liu, H. W.; Xue, Q. J. Preparation and Characterization of Electrochemically Deposited Carbon Nitride Films on Silicon Substrate. *J. Phys. D: Appl. Phys.* **2004**, *37*, 907−913.
(35) Biesinger, M. C.; Payne, B. P.; Grosvenor, A. P.; Lau, L. W. M.; Gerson, A. R.; Smart, R. S. C. Resolving Surface Chemical States in XPS Analysis of First Row Transition Metals, Oxides and Hydroxides: Cr, Mn, Fe, Co and Ni. *Appl. Surf. Sci.* **2011**, *257*, 2717−2730.
(36) Petitto, S. C.; Marsh, E. M.; Carson, G. A.; Langell, M. A. Cobalt Oxide Surface Chemistry: The Interaction of CoO, Co_3O_4 and Co_3O_4 with Oxygen and Water. *J. Mol. Catal. A: Chem.* **2008**, *281*, 49−58.
(37) Wagner, C. D.; Riggs, W. M.; Davis, L. E.; Moulder, J. F.; Muilenberg, G. E. *Handbook of X-ray Photoelectron Spectroscopy*, 1st ed.; Perkin-Elmer Corp., Physical Electronics Division: Eden Prairie, MN, 1979.
(38) Prabhakaran, K.; Ogino, T. Behavior of Ultrathin Layers of Co on Si and Ge Systems. *Appl. Surf. Sci.* **1996**, *100−101*, 518−521.
(39) Lu, C.-E.; Pu, N.-W.; Hou, K.-H.; Tseng, C.-C.; Ger, M.-D. The Effect of Formic Acid Concentration on the Conductivity and Corrosion Resistance of Chromium Carbide Coatings Electroplated with Trivalent Chromium. *Appl. Surf. Sci.* **2013**, *282*, 544−551.
(40) Stypula, B.; Stoch, J. The Characterization of Passive Films on Chromium Electrodes by XPS. *Corros. Sci.* **1994**, *36*, 2159−2167.
(41) Jiang, T.; Wallinder, I. O.; Herting, G. Chemical Stability of Chromium Carbide and Chromium Nitride Powders Compared with Chromium Metal in Synthetic Biological Solutions. *ISRN Corros.* **2012**, *2012*, 10.
(42) Bethune, D. S.; Klang, C. H.; de Vries, M. S.; Gorman, G.; Savoy, R.; Vazquez, J.; Beyers, R. Cobalt-Catalysed Growth of Carbon Nanotubes with Single-Atomic-Layer Walls. *Nature* **1993**, *363*, 605−607.
(43) Tritsaris, G. A.; Mathioudakis, C.; Kelires, P. C.; Kaxiras, E. Optical and Elastic Properties of Diamond-Like Carbon with Metallic Inclusions: A Theoretical Study. *J. Appl. Phys.* **2012**, *112*, 103503.
(44) Ferrari, A. C.; Robertson, J. Raman Spectroscopy of Amorphous, Nanostructured, Diamond-Like Carbon, and Nanodiamond. *Philos. Trans. R. Soc., A* **2004**, *362*, 2477−2512.
(45) Ferrari, A. C.; Robertson, J. Interpretation of Raman Spectra of Disordered and Amorphous Carbon. *Phys. Rev. B: Condens. Matter Mater. Phys.* **2000**, *61*, 14095−14107.
(46) Ferrari, A.; Robertson, J. Resonant Raman Spectroscopy of Disordered, Amorphous, and Diamond-Like Carbon. *Phys. Rev. B: Condens. Matter Mater. Phys.* **2001**, *64*, 075414.
(47) Yen, B. K.; White, R. L.; Waltman, R. J.; Mate, C. M.; Sonobe, Y.; Marchon, B. Coverage and Properties of a-SiN_x Hard Disk Overcoat. *J. Appl. Phys.* **2003**, *93*, 8704−8706.